The Aeronautical Journal (2023), 1–24
doi:10.1017/aer.2023.111

ROYAL AERONAUTICAL SOCIETY

REGULAR PAPER

Thermal management system design for a series hybrid-electric propulsion architecture

M. Potamiti , V.G. Gkoutzamanis and A.I. Kalfas

Department of Mechanical Engineering, Laboratory of Fluid Mechanics and Turbomachinery, Aristotle University of Thessaloniki, Thessaloniki, GR, Greece
Corresponding author: V. G. Gkoutzamanis; Email: vgkoutzam@meng.auth.gr

Received: 15 May 2023; **Revised:** 25 September 2023; **Accepted:** 25 October 2023

Keywords: series hybrid propulsion architecture; decentralised thermal management system; centralised thermal management system; liquid-based thermal management system

Abstract

The current paper is focused on the conceptual design of a thermal management system with a liquid working medium for a commuter hybrid-electric aircraft, featuring a series propulsion configuration. Regarding the system's architecture, parametric analyses are conducted, by altering the number of heat exchangers. To clarify, a centralised and a decentralised thermal management system architecture are examined. Furthermore, a computational model calculates the temperatures during the system's operation and the required coolant mass flows to sufficiently cool all the compartments. Subsequently, the required heat exchanger surface is determined and the weight of each compartment that comprises the thermal management system can be calculated. It is worth noting, that the compartments' cold plate weight is integrated. The results indicate that the decentralised configuration results in lower temperature fields for all components compared to the centralised configuration. However, the latter weighs 32.2% lower at 158.22kg while the decentralised configuration weighs 233.48kg.

Nomenclature

Symbols

NTU	number of transfer units	–
U	heat transfer coefficient	W/m^{2}K
A	heat transfer area	m^2
C_r	specific heat capacity ratio	–
C_{min}	minimum specific heat capacity	kJ/kg/K
ΔP	pressure drop	bar
$\dot{m}$	mass flow rate	kg/s
D_H	hydraulic diameter	mm
L	pipes length	mm
f	friction factor	–
W	weight	kg
V	volume	m^3

Subscripts

conv	convection
cool	coolant
res	reservoir
bat	battery

Greek Symbols

β	compactness ratio	m^2/m^3
ε	heat exchanger effectiveness	–
σ	porosity	–

Abbreviations

CDTO	cold day takeoff
CHEX	compact heat exchanger
CP	cold plate
CTMS	centralised thermal management system
ECS	environmental control system
EGW	ethylene glycol water mixture
EM	electric motor
EPS	electrical power system
DTMS	decentralised thermal management system
HEX	heat exchanger
HDTO	hot day takeoff
LH_2	liquified hydrogen
LHT	liquid hydrogen tank
PAO	polyalphaolefin
PGW	propylene glycol and water mixture
PMAD	power management and distribution center
TMS	thermal management system

Trade Names

Pycharm	programming environment
Python	programming language

1.0. Introduction

The aviation sector is responsible for approximately 5% of anthropogenic causes of climate change. In this direction the Advisory Council for Aviation Research and Innovation (ACARE) has set a goal to reduce the CO_2 by 75% for each passenger per kilometer, as well as the reduction of NO_x and noise emissions by 90% and 65% respectively, by the year of 2050 [1, 2]. This is the driving force to research the exploitation of alternative energy sources to supply hybrid propulsion concepts, such as electric energy, liquified hydrogen (LH_2) and liquified natural gas.

Electric propulsion architectures are classified into all electric, hybrid and turboelectric [3, 4]. All electric aircraft employ batteries for thrust generation, which limits their range due to the inherent limitations of reduced gravimetric energy, compared to the jet fuel counterpart [5]. Hybrid electric configurations use gas turbine engines for propulsion and to charge batteries. They can be classified into parallel, series and series/parallel partial hybrid layouts. On a parallel configuration either or both the battery powered motor and the gas turbine can provide propulsive power. Parallel hybrid configurations have been extensively studied in the literature, with applications on commuter and regional classes [6–11]. Their apparent benefits include easier implementation, reduced complexity and costs, compared to the other variants. Series hybrid configurations, on the other hand, allow for the decoupling of electrical and thermal propulsors and enable novel configurations based on distributed propulsion. The generator driven by the gas turbine provides power to the motors and charges the batteries. The series/parallel architecture has either one or more fans which can be driven by a gas turbine (GT) while other fans are driven exclusively by electrical motors. The series architecture is normally an enabler of

https://doi.org/10.1017/aer.2023.111 Published online by Cambridge University Press

distributed propulsion concepts [12]. In this direction, turboelectric propulsion also explores the benefit of distributed propulsion, which reduces aerodynamic drag [13–15]. It is based on a GT linked with a generator which then powers electric motors (EMs), and can be characterised as fully turboelectric and partial. Partial turboelectric propulsion, a portion of propulsive power is produced using electric propulsion, while the rest is produced by a GT. In addition, the use of cryogenic fuels is researched, such as LH_2. However, this configuration poses a challenge as the voluminous cylindrical fuel tanks need to be accommodated.

As mentioned above, electric propulsion components do not employ a natural exhaust system like GT engines. Therefore, a thermal management system (TMS) must be incorporated to sufficiently cool electric compartments, but it is of primary importance to be as light as possible to minimise its integration impact on the aircraft. To design the TMS, a suitable working medium must be selected [16–18], including ram air. Architectures utilising air are deemed simpler and safer [19]. To improve their efficiency, added ducting could be used, cooling each compartment individually. Moreover, heat sinks could be applied on the compartments, to further benefit from the air convection. Furthermore, liquid working medium could be utilised, such as water, water and propylene glycol (PGW), or ethylene glycol, or glycol mixtures [20–22], polyalphaolefin (PAO) [23, 24] and jet fuel [25]. These thermal management architectures provide high efficiency but also high integration impact, and are classified as centralised and decentralised. In centralised systems, the compartments are cooled via a central heat exchanger (HEX), while in decentralised systems individual cooling loops are designed for each compartment. Centralised systems feature either a series architecture or a parallel. In a series architecture all the environmental control system (ECS) compartments are cooled successively, which leads to some compartments being cooled by higher temperature liquid. On a parallel architecture, different loops are designed to cool a ECS compartment or a group of compartments which are then all connected in parallel. To further improve heat transfer either puller fans or a Brayton cooling cycle can be applied [26]. In addition, phase change materials (PCMs), such as Mg, Urea-KCL [27], can be attached to the external surface of a battery stator, as they feature measurable latent heat. Furthermore, in lighter aircraft surface heat exchangers can provide the same magnitude of cooling with a conventional TMS [28].

Li-ion type batteries introduce significant temperature sensitivity. In low temperatures, (below $-10°C$) they present charging resistance, whereas at temperatures higher than $40°C$, their power is depleted [29]. Also, differentiation in temperature distribution above $5°C$, alters their electrochemical efficiency. Consequently, their cold plates (CPs) design is investigated. In some cases, CPs could feature micro-channels to increase heat transfer. Furthermore, placing the CPs on their smaller latent surfaces, renders them lighter and more economic [30]. To achieve more effective cooling, separate cooling loops for batteries can be designed, even with different liquid medium such as silicone (PSF-5), PCMs or water mixture with AL_2O_3 nanoparticles [31, 32]. This mixture features high heat transfer efficiency.

As the majority of research focuses mainly on parallel-hybrid configurations [8–11], the motivation of this work is to explore the preliminary design of a TMS considering a series propulsion architecture. Different thermal management architectures are examined, by altering the number of the system's heat exchangers. Comparing these architectures for a set propulsion design, enables the selection of the most efficient solution, while allowing to examine the novel concept of applying the simpler, series propulsion architecture on hybrid electric propulsion systems. To achieve the goals of this study, a low-fidelity thermal model is developed. The model is capable of sizing the heat exchangers and calculates the temperatures and required coolant mass flows for each point of the system. For the analyses executed, the cooling medium selected is water and propylene glycol mixture 50% (PGW50). Furthermore, the weight of each model as well as their respective compartments are calculated.

2.0. Methodology

2.1. Propulsion configuration and assumptions

The propulsion architecture is based on one of the configurations developed in the Clean Sky 2 European project HECARRUS (Hybrid ElectriC smAll commuteR aiRcraft conceptual design). The aircraft is

https://doi.org/10.1017/aer.2023.111 Published online by Cambridge University Press

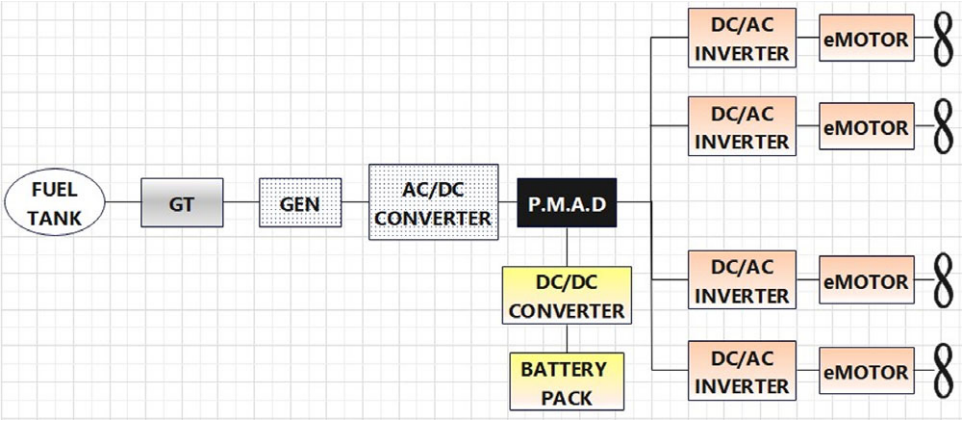

Figure 1. *Propulsion architecture schematic.*

designed to carry up to 19 passengers and executes small range flights, employing technologies applicable by 2030 and beyond. The selected propulsive architecture features a series hybrid configuration, and it is illustrated on Fig. 1. The propulsive layout is composed of four electric motors, two on each wing. The gas turbine is embedded in the aft part of the aircraft's fuselage. It is exclusively connected to the generator and is assumed to provide approximately 1,100kW of power. The generator is connected both with the batteries and the power management and distribution system (PMAD) in order to drive the motors. The batteries, which provide 1,600kW of power, are also linked with the PMAD, to provide propulsive power to the motors. The motors' power is 600kW, so the electrical power system (EPS) produces 2.4MW of power.

The mission executed by the aircraft is constituted by the following segments: taxi-out, takeoff, climb, cruise, descend, landing and taxi-in. Batteries supply propulsive power during takeoff and climb. Additionally, they should contribute supplementary power in case of a motor failure. During cruise, the batteries can be charged with the generator's surplus of power. The TMS is designed during the mission segment where the higher thermal loads are expected, and therefore the EPS's function is exacerbated. In the context of this paper this occurs during takeoff, and the functional parameters of each compartment at this point are presented on Table 1. The lower temperature limit constraint is enforced by the Li-ion batteries that must function at 40°C.

The TMS development relies on two axes: (1) provide sufficient cooling of EPS compartments to ensure safe function and (2) enable lightweight design. The working medium selected must fulfill certain criteria as following:

i. Good thermophysical properties: high thermal conductivity, low freezing point and explosion point for safe storage.
ii. High boiling point, low freezing point and bursting point for safe storage.
iii. Thermal and chemical stability.
iv. High life expectancy without the need for added chemicals.
v. Non-corrosive.
vi. Environmentally friendly, nontoxic.
vii. Cost effective and vastly available.
viii. High autoinflammation point.

Considering the requirements above, a qualified working medium is the propylene glycol mixture. In this respect, the fluid selected is a propylene glycol and water mixture, with 50% mix ratio. About

https://doi.org/10.1017/aer.2023.111 Published online by Cambridge University Press

Table 1. *Compartment thermal limits, power outputs and thermal loads*

EPS compartment	Limit temperature (°C)	Power output (kW)	Thermal load (kW)	Efficiency (%)
eMotor	100	600	24	96
DC/AC inverter	65	600	6	99
Generator	100	1,100	55	95
AC/DC converter	65	1,100	11	99
Battery pack	40	1,600	48	97
DC/DC converter	65	1,600	16	99

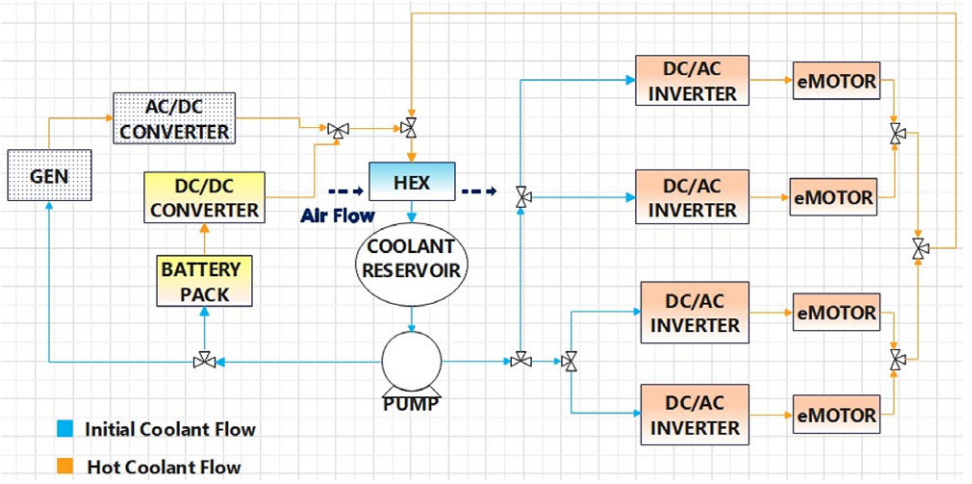

Figure 2. *Centralised TMS architecture.*

the TMS architecture, two layouts are developed to compare their integration impact on the aircraft: a centralised as well as a decentralised arrangement.

In the centralised architecture the total working liquid flow is cooled in a central heat exchanger via ram air, as illustrated on Fig. 2. However, in the decentralised arrangement each individual liquid flow is cooled on each loop with a separate heat exchanger, as presented on Fig. 3. Consequently six heat exchangers are employed. Essentially, these two systems represent the two extreme cases from a totally isolated to a fully redundant system. Thus, the latter is deemed safer, as it ensures that if any of the HEXs fail, the other compartments will remain sufficiently cooled. From the figures provided, it is concluded that apart from the differentiation in the number of HEXs, the architectures are similar. The working medium exits the tank and is pumped to six different routes, connected in parallel. In the first loop, the generator and AC/DC converter are cooled. On the second loop the batteries and their DC/DC converter are cooled. Furthermore, one loop is designed for every motor and DC/AC inverter pair.

The heat exchangers considered in this report are of the compact crossflow HEX type with both fluids unmixed. Compact heat exchangers (CHEXs) are characterised by surface density β higher than $700 m^2/m^3$, and combine small weight as they feature the smaller possible volume, but also high efficiency [33, 34]. For the heat exchanger dimensioning the effectiveness (ε) – number of transfer units (NTU), as it facilitates the calculation of the outlet temperatures of fluids. The NTU and the effectiveness for a crossflow heat exchanger with both fluids unmixed are defined as follows from Equations (1)–(3):

$$\varepsilon = 1 - \exp\left(C_r NTU^{0.22} \cdot \exp\left(-C_r NTU^{0.78}\right) - 1\right) \quad (1)$$

https://doi.org/10.1017/aer.2023.111 Published online by Cambridge University Press

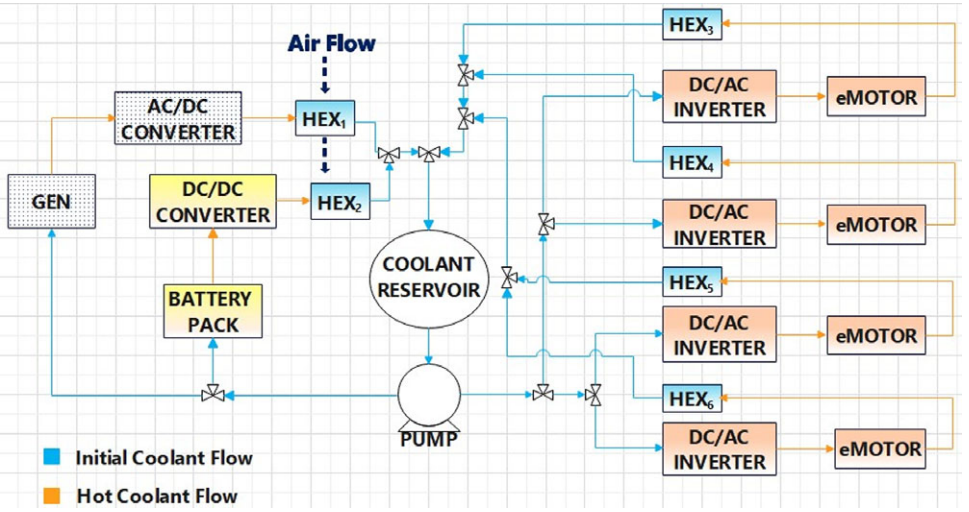

Figure 3. *Decentralised TMS architecture.*

$$\varepsilon = 1 - e^{\left(C_r NTU^{0.22}\left(e^{-C_r NTU^{0.78}} - 1\right)\right)} \tag{2}$$

$$NTU = \frac{UA}{C_{\min}} \tag{3}$$

In order to design the heat exchanger, the values required are:

- The working medium on both the hot and cold side.
- Inlet and outlet temperatures for one working medium.
- The thermal conductivity of each fluid.
- Either the outlet or the inlet temperature of the other fluid.
- An initial estimation for the total heat transfer coefficient U.

To assume the value of the total heat transfer coefficient, bibliographic research was conducted. In the work of Mortean et al. [35]. Experimental testing on polymer CHEX was executed, to assess its performance, resulted in heat transfer coefficient with values 70–194, with varying Re number. Regarding CHEXs employing water and Al_2O_3 nanoparticles [36], their U ranges from 150–200W/(m^2K), depending on the mix ratio. This study further highlights this mixture's high cooling capacity in comparison to water and EGW as presented on Fig. 4.

Furthermore, the performance analysis of plate fin CHEXs with conventional and improved rectangular, as well as twisted fins was studied [37]. As the fins design is not explored during this research, regular fins, as non-improved fins were considered, to account for the most exacerbated CHEX efficiency. In this case, the U ranged from 168 to 224W/(m^2K). In addition, in an application where an aluminum CHEX is employed for gas-turbine plant of power 3.7MW [34], with air and water, similar working mediums as the heat exchangers of the current research, the U was calculated 166W/(m^2K). This value was selected to dimension this paper's heat exchangers and all the values considered are presented on Table 2. It is also worth highlighting that other values were also examined but did not significantly alter the analysis results. Consequently, the coefficient's impact on the results is considered minor.

https://doi.org/10.1017/aer.2023.111 Published online by Cambridge University Press

Table 2. *Heat transfer coefficient values*

Heat transfer coefficient ($W/(m^2K)$)	References
70–194	[35]
150–200	[36]
168–224	[37]

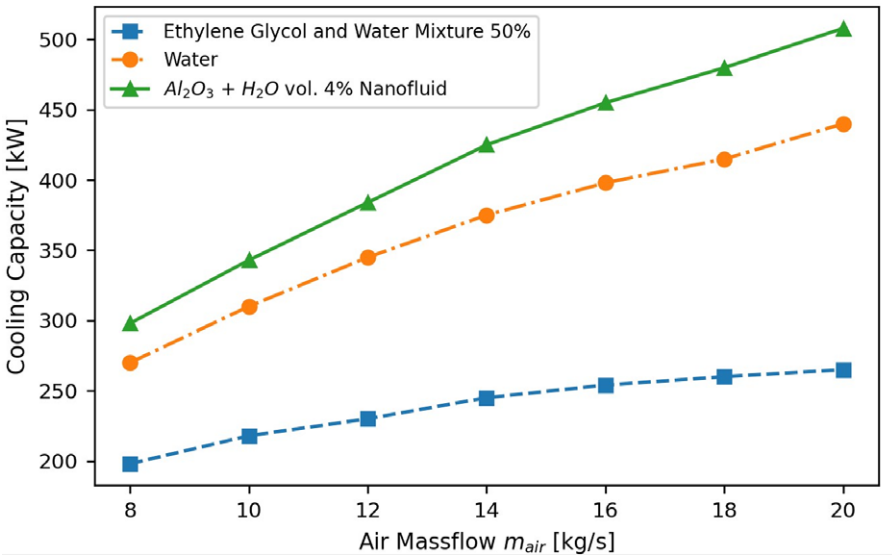

Figure 4. *Cooling capacity of various water-based coolants [35].*

2.2. Computational model development

To define the necessary functional parameters as well as the weight of the TMS, a computational model, consisting of two parts, is developed. The first part, the thermal model, calculates the minimum required HEX area. Afterwards, the weight model extracts the TMS compartments' weights.

The computational model is compiled in Python, utilising the integrated development environment of Pycharm. Vital for its function is the use of numpy library as it allows to examine a range of values at once. Furthermore, with matplotlib library the results are plotted to draw conclusions. In an attempt to render the computational model in a more user-friendly manner, widgets are developed with tkinter library.

2.2.1. Thermal model

In order to dimension the HEXs, which is the objective of the thermal model, appropriate assumptions must be considered, regarding their performance. In this research, the whole heat transfer coefficient is $166 W/m^2K$, and the efficiency of every HEX is assumed to be 0.95. Furthermore, the heat loads that the HEXs receive must be calculated. To achieve this, two heat loading scenarios are examined. Referring to the first, the conduction between the cooling fluid and each compartment. The second case considers the convection between the CP surface and its surrounding air, which is at 22.7°C and the heat transfer coefficient is estimated $30.68 W/m^2K$ [21]. The thermal loads are calculated from the formulas as follows.

$$Q_{\text{total}} = Q_{\text{cond}} + Q_{\text{conv}} \tag{4}$$

https://doi.org/10.1017/aer.2023.111 Published online by Cambridge University Press

Table 3. *Cold plate surfaces*

EPS compartment	Cold plates surface (m^2)
eMotor	0.49
DC/AC inverter	0.49
Generator	1.07
AC/DC converter	1.07
Battery pack	3.96
DC/DC converter	1.22

$$Q_{\text{cond}} = k \cdot (T_{\text{lim}} - T_{\text{air}}) \tag{5}$$

$$Q_{\text{conv}} = (1 - n) \cdot P \tag{6}$$

The cold plates surface for each propulsion compartment are presented on Table 3.

To execute the thermal computational model, the atmospheric conditions must be defined. The TMS's design point is selected during the takeoff phase at sea level, where the highest EPS thermal loads are expected. In addition, as batteries feature elevated thermal sensitivity, three different atmosphere models are investigated. The baseline model implements an ECS, in order to regulate the ram air temperature at 7°C. The two alternative models examine hot (HDTO) as well as cold (CDTO) takeoff conditions, where the air's temperature is 40°C and −10°C, respectively. As the atmospheric conditions are determined, the coolant mass flows as well as the temperatures for each point of the TMS can be computed. It is worth highlighting that propylene glycol thermophysical properties are obtained using the library pyfluids.

In reference to the centralised TMS (CTMS), utilising the energy equilibrium for the cold fluid, the air, and the hot, propylene glycol, the inlet and outlet temperatures for the cold and hot side can be calculated. Furthermore, the whole required coolant mass flow is defined. After the central HEX is sized, the mass flow of each loop and the temperatures of each compartment, are calculated from the energy equilibrium of ach compartment as presented below. While defining the operation temperatures in each loop, the inlet temperature of the coolant in the HEX is re-calculated. Subsequently a convergence criterion is introduced, so that the initial and final value of this temperature are equal.

On the decentralised TMS (DTMS) six HEXs must be sized, although it is considered that they are all cooled with the same air mass flow and feature the same performance characteristics. While on the centralised model, the whole mass flow is defined in the starting point of the cooling loop, the opposite occurs on the decentralised model. As both the inlet and outlet temperatures are defined for each HEX, the coolant mass flow of each cooling loop is computed. Consequently, the temperatures of each compartment are calculated and lastly the initial temperature of the coolant and the cumulative coolant mass flow. It is necessary to note that in this case, the convergence criterion, while expressed as in the centralised model, refers to each HEX separately. Therefore, three convergence criteria must be fulfilled. In addition, for both models, sensitivity analyses are conducted, for a range of inlet ram air mass flow and HEXs heat transfer surfaces. The goal is to minimise the heat transfer surface while ensuring safe operation of each compartment.

2.2.2. Weight model

With the completion of the thermal computational model, the heat transfer surface of each hex is defined, and necessary coolant mass flows. Subsequently the weight of each compartment can be calculated. Utilising the definition of the compressibility ratio, the HEX volume is derived from the following equation:

https://doi.org/10.1017/aer.2023.111 Published online by Cambridge University Press

$$V_{HEX} = \frac{A_{HEX}}{\beta} \tag{7}$$

Consequently, the dry weight can be calculated from Equation (8), and the wet weight from Equation (9), considering that HEXs are constructed from aluminum. It is important to calculate both, as wet weight includes the coolant, with the assumption that 25% of porosity accounts for the liquid coolant channels. The above methodology for CHEX sizing is also presented in previous research of Gkoutzamanis et al. [21].

$$(W_{HEX})_{dry} = V_{HEX} \cdot \rho_{HEX} \cdot (1 - \sigma) \tag{8}$$

$$(W_{HEX})_{wet} = (W_{HEX})_{dry} + V_{HEX} \cdot \frac{1}{4} \cdot \sigma \cdot \rho_{coolant} \tag{9}$$

Piping Weight

The piping system is comprised of the required routes to sufficiently cool the EPS compartments. One route is designed to cool the generator and its AC/DC converter, another for the battery pack and DC/DC converter and one for each motor and DC/AC inverter pair. The piping weight depends on the hydraulic diameter, which is considered 18 mm at all routes. In addition, the piping length is estimated from a preliminary CAD drawing. The wall thickness of the pipes is considered 1mm.

Pump power and weight

The pump's purpose is to recover the liquid's pressure loss during its circulation in all of the cooling loops. Pressure loss occurs both in the pipes and the EPS compartments. The piping pressure loss is calculated on each loop individually. The generator loop comprises 15% of piping, the battery pack loop 10% and each motor loop 17.5%, on both TMS architectures exists a joint route where the liquid coolant enters its reservoir, and is afterwards driven through the pump in the system. This route comprises 5% of the whole length. Therefore, the pipes pressure loss is derived from Equation (10).

$$(\Delta P_{pipe})_{tot} = (\Delta P_{pipe})_{bat} + (\Delta P_{pipe})_{gen} + (\Delta P_{pipe})_{m} + (\Delta P_{pipe})_{joint} \tag{10}$$

Furthermore, for each route the pressure loss is dependent on the Darcy-Weisbach friction factor, and the liquid's velocity. To calculate the friction factor empirical equations, like Colebrook-White are employed, according to Reynolds number. The EPS compartments pressure loss however, is derived from empirical data [21, 33]. In both TMS designs the HEXs pressure loss is 2 bar, because of their narrow liquid channels. The other compartments feature a summed-up pressure loss of approximately 4 bar. Subsequently the compartments and the TMS pressure loss are defined from Equation (11).

$$(\Delta P_{TMS}) = (\Delta P_{pipe})_{tot} + (\Delta P_{comp})_{tot} \tag{11}$$

The pump considered in this research is a rotodynamic, centrifugal kind. Its power can be derived from pressure loss through Equation (12), with the assumption that the impeller's efficiency is 0.7 [38].

$$P_{pump} = \frac{\Delta P_{TMS} \cdot (\frac{\dot{m}}{\rho})_{coolant}}{n_{imp} \cdot n_{inv} \cdot n_{m}} \tag{12}$$

3.0. Results

3.1. Thermal model results

The central HEX of the TMS must be capable of dissipating a thermal load of approximately 250kW. To realise the minimum heat transfer HEX area required, sensitivity analyses are conducted for a range of ram air mass flows and HEX surface areas. The range of these parameters is presented in Table 4, and it is applied to all three atmospheric conditions: controlled by ECS, HDTO, CDTO. In addition, the effect of surrounding air convection is examined.

Regarding the DTMS, each HEX receives the thermal load of the compartments in the cooling loop it is placed. The lowest thermal load occurs on the motor loop at 30kW, while the battery and generator

https://doi.org/10.1017/aer.2023.111 Published online by Cambridge University Press

Table 4. *Parameters examined on sensitivity analyses*

Functional parameter	CTMS range	DTMS range
HEX_1 heat transfer area (m^2)	50–200	10–55
HEX_2 heat transfer area (m^2)	–	10–55
$HEX_{3\text{-}6}$ heat transfer area (m^2)	–	5–50
Air mass flow (kg/s)	5–30	2–20

loops receive similar loads at 64 and 66kW, respectively. The range of the parameters examined are presented on Table 4, and as each HEX receives different heat loads, different heat transfer surface ranges are investigated.

While on the CTMS the strictest design constraint is imposed by the battery pack temperature that needs to be maintained at 40°C, on the DTMS more factors contribute. As each HEX is placed on a cooling loop, its design is affected by the compartment with the strictest temperature limit. On the generator and motor loops the compartments setting the limit temperature are the AC/DC converter and DC/AC inverter, respectively. The battery loop is restrained by the battery at 40°C.

3.2. Environmental control system conditions

3.2.1. Centralised thermal management system

In Fig. 5, the inlet and outlet temperature of liquid coolant in HEX hot side are featured, including PGW50's boiling point at 106,5°C, as temperatures must not surpass that. It is evident that higher air mass flow leads to lower temperatures. However higher heat transfer areas lead to increased temperatures.

The liquid coolant mass flow, presented on Fig. 6, demonstrates opposite trends, as it increases with higher air mass flow, and decreases with higher heat transfer area. Consequently, there exists a trade-off between heat transfer area and coolant mass flow. Furthermore, sensitivity analyses showcase that coolant mass flows higher than 2.8kg/s, exponentially increase pump weight.

The coolant temperature exiting the battery pack, essentially configures the HEX's design space, as batteries must function below 40°C. This constraint is presented on Fig. 7, showcasing the outlet coolant temperature on batteries.

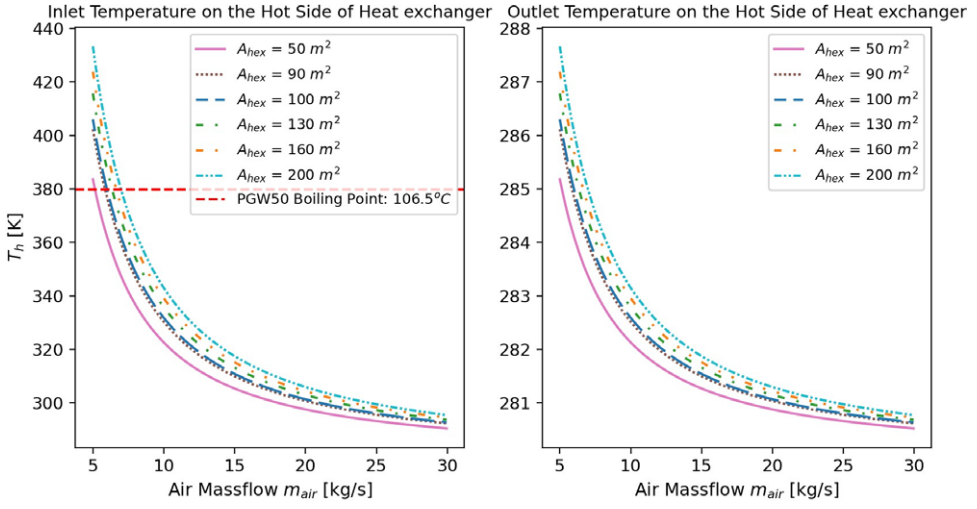

Figure 5. *Inlet and outlet temperature on hot side of heat exchangers, ECS conditions, CTMS.*

https://doi.org/10.1017/aer.2023.111 Published online by Cambridge University Press

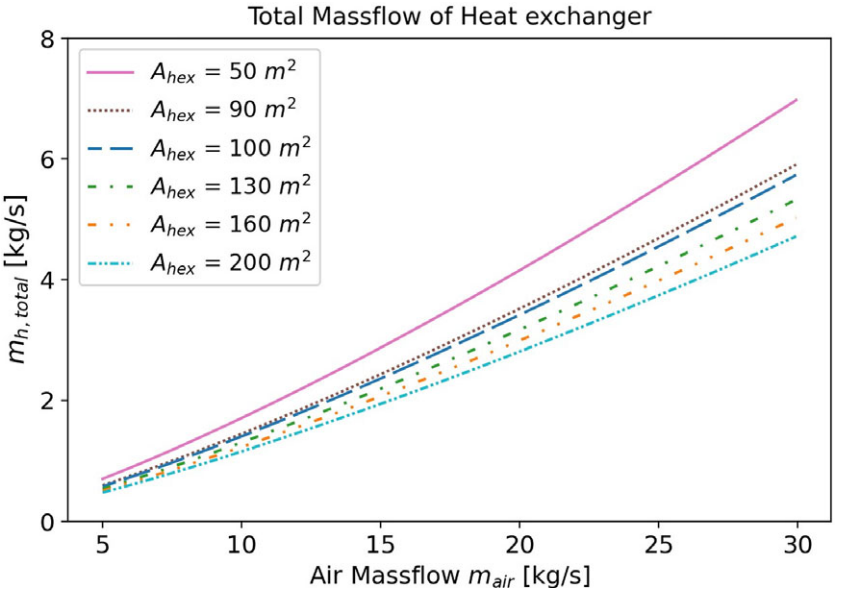

Figure 6. *Total required coolant mass flow, ECS conditions, CTMS.*

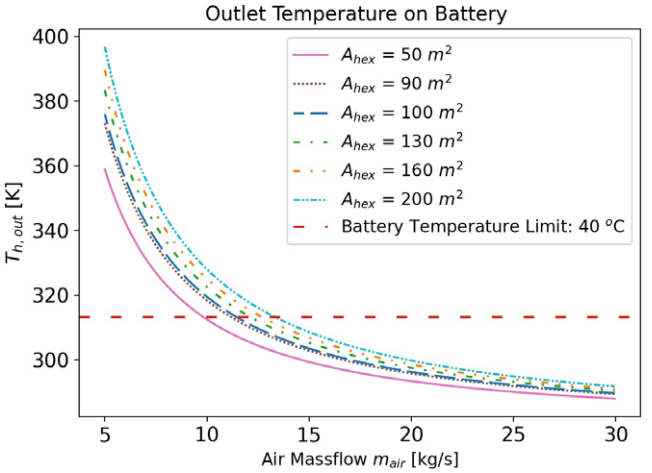

Figure 7. *Outlet coolant temperature on battery, ECS conditions, CTMS.*

Considering the constraints analysed above, the selected values for the configuration, regarding ECS ram air conditions, feature 95m^2 HEX area and 11.38kg/s air mass flow, which yield 1.68kg/s coolant mass flow. The results are presented on Table 5.

Decentralised thermal management system

As mentioned, each HEX of the decentralised design is affected by different constraints. Subsequently to determine each HEX's heat transfer surface, sensitivity analyses were conducted, considering only its individual limitations in respect to the design. The results of the exploration regarding inlet temperatures of each HEX and the outlet battery temperature are presented in Fig. 8. It is evident that higher temperatures occurate the generator and battery loop, and the strictest sizing limitation is set by the outlet coolant temperature on the batteries.

https://doi.org/10.1017/aer.2023.111 Published online by Cambridge University Press

Table 5. *TMS sensitivity analysis results for ECS conditions*

Parameter	CTMS value	DTMS value
HEX_1 heat transfer area (m^2)	95	22
HEX_2 heat transfer area (m^2)	–	20
$HEX_{3\text{-}6}$ heat transfer area (m^2)	–	15
Air mass flow (kg/s)	11.38	2.76
Coolant mass flow (kg/s)	1.168	4.78
$T_{hout,bat}$ (K)	312.98	312.87

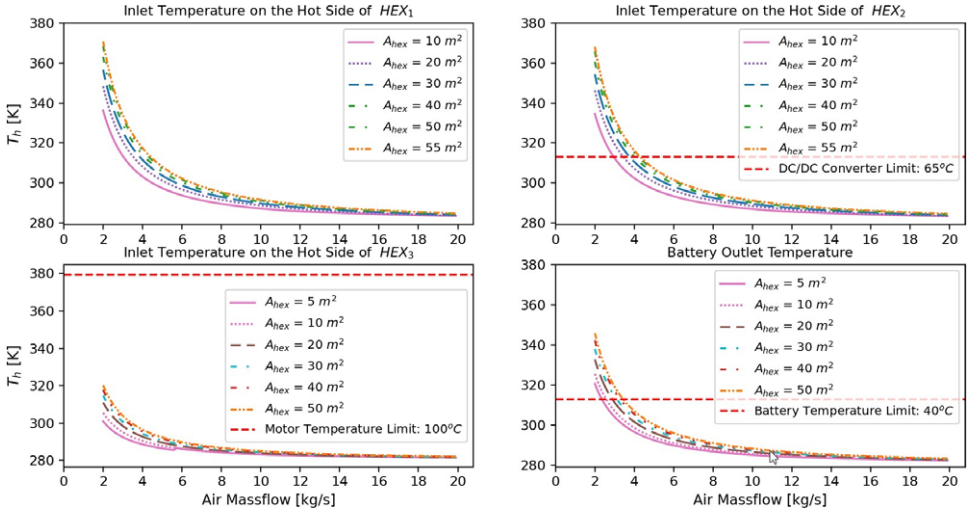

Figure 8. *Inlet temperatures on each HEX and outlet coolant temperature sensitivity analyses, DTMS.*

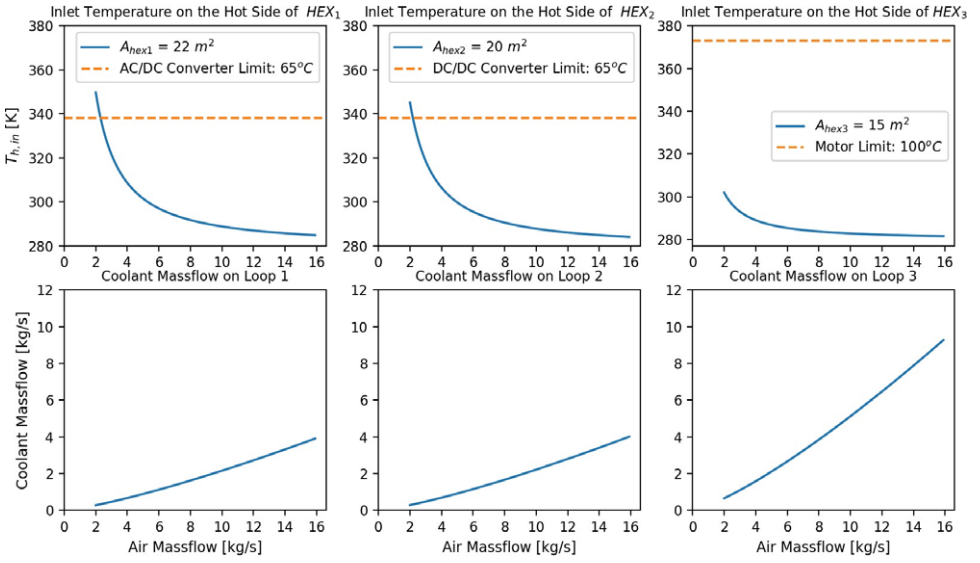

Figure 9. *Inlet temperature on hot side and required coolant mass flow of each heat exchanger, ECS conditions, DTMS.*

https://doi.org/10.1017/aer.2023.111 Published online by Cambridge University Press

In conclusion, the surface of the generator loop HEX is 22m^2, the battery 20m^2, and for each motor loop 15m^2. As the HEXs heat transfer surfaces are selected, further sensitivity analysis, considering the whole TMS and convergence criteria set, are executed, to determine the required air and coolant mass flow. The temperature limits set for each cooling loop are presented on Fig. 9, where the outlet temperature of the coolant on each compartment is plotted. It is apparent from the required coolant mass flows on each loop that the motor and inverter loop need the highest mass flow. As there are four similar loops total this phenomenon exacerbates the value of the total coolant mass flow.

3.2.2. Hot day takeoff conditions

Centralised thermal management system

Assuming HDTO conditions, 40°C air is utilised to cool the HEX. Observing the temperature trends, a 5% increase can be realised. As mentioned above the battery pack's temperature determines the viable design space for the HEX. On Fig. 10, presenting the coolant outlet temperature in battery pack, it is illuminated that a 40°C working temperature is unachievable even for extreme air mass flow values, for HDTO conditions. However, either attaching PCMs on the batteries or designing a separate cooling loop using a higher performance freezing liquid, could improve their temperature fields. Furthermore Lithium-sulphur (Li-S) batteries could further extend the operating temperature range, as this type of battery can operate at temperatures of up to 70°C [39].

Subsequently, a higher limitation is examined, at 45°C, which requires air mass flow higher than 40kg/s. Such elevated air mass flow values, induce a ram-air drag, hence a limitation at 50°C is further investigated, which results in 29.18kg/s air mass flow. Hence this temperature limitation is selected, as presented on Table 6 and the necessary coolant mass flow is 5.63kg/s, which is 70% more than the mass flow at ECS conditions.

Decentralised thermal management system

At hot day takeoff conditions, the strictest requirement as mentioned above is outlet coolant temperature on battery as presented on Fig. 11.

As it occurred on the CTMS, the 40°C limit for safe battery operation is surpassed, as the required mass air mass flow must be further than 50kg/s. However, when the limit is adjusted to 50°C, the required air mass flow is 6.98kg/s, and the corresponding coolant mass flow is 15.75kg/s as illustrated on Table 6, which would greatly impact the pump mass.

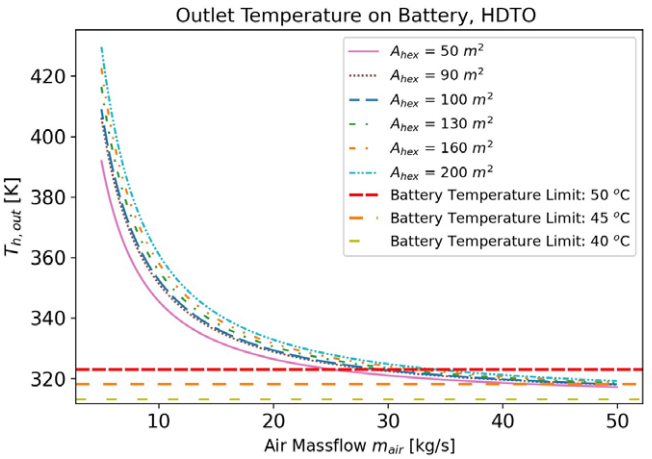

Figure 10. *Outlet coolant temperature on battery, HDTO conditions, CTMS.*

https://doi.org/10.1017/aer.2023.111 Published online by Cambridge University Press

Table 6. *TMS sensitivity analysis results for HDTO conditions*

Parameter	CTMS value	DTMS value
Air mass flow (kg/s)	29.18	6.98
Coolant mass flow (kg/s)	5.63	15.75
$T_{hout,bat}$ (K)	322.97	322.98

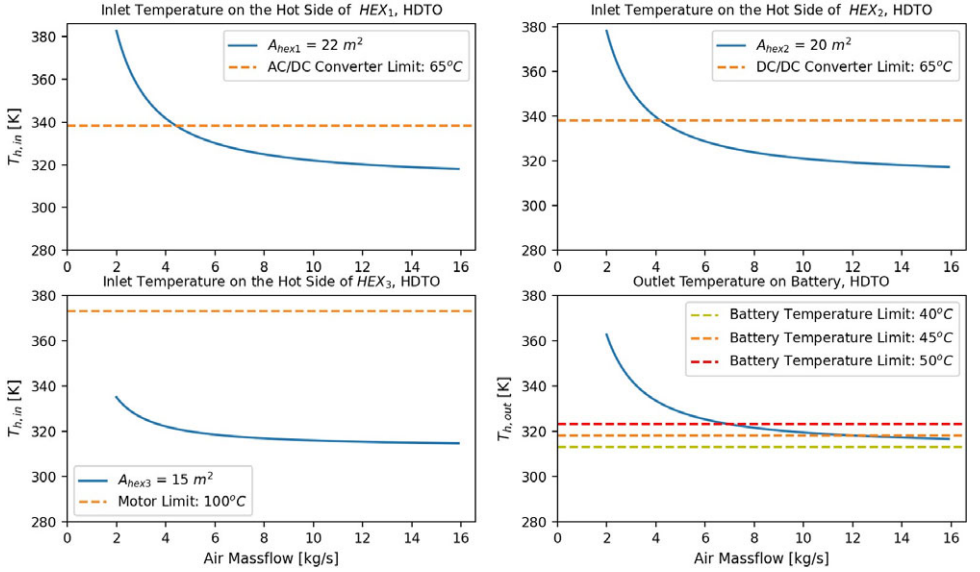

Figure. 11. *Inlet temperature on hot side and required coolant mass flow of each heat exchanger, HDTO conditions, DTMS.*

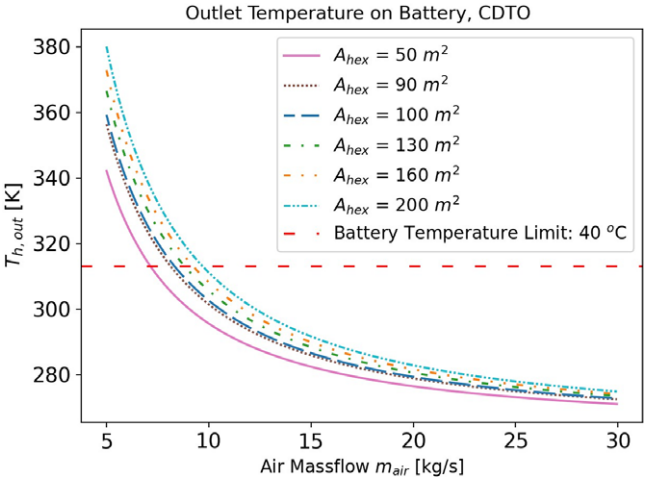

Figure 12. *Outlet coolant temperature on battery, CDTO conditions, CTMS.*

https://doi.org/10.1017/aer.2023.111 Published online by Cambridge University Press

Table 7. *TMS sensitivity analysis results for CDTO conditions*

Parameter	CTMS value	DTMS value
Air mass flow (kg/s)	8.25	1.99
Coolant mass flow (kg/s)	1.11	3.16
$T_{hout,bat}$ (K)	312.97	312.98

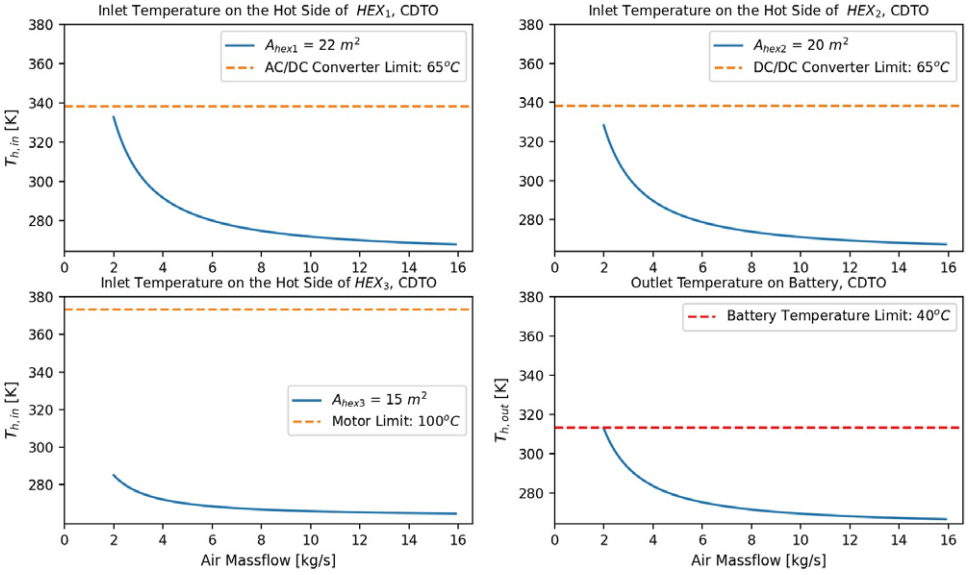

Figure 13. *Inlet temperature on hot side and required coolant mass flow of each heat exchanger, CDTO conditions, DTMS.*

3.2.3. Cold day takeoff conditions

Centralised thermal management system

At CDTO conditions, which occur at −10°C, operational temperatures decrease approximately by 5%, compared to ECS conditions. This can expand the viable design space for the HEX. Furthermore, except of the upper temperature limit for the battery pack at 40°C, a lower limit is introduced at −10°C, as their power is depleted. These constraints are presented at Fig. 12, where it is evident that all temperatures are higher than the lower limit.

Accounting all design constraints and HEX transfer surface, the air mass flow selected is 8.25kg/s as presented on Table 7. In addition, the corresponding coolant mass flow is 1.11kg/s.

Decentralised thermal management system

At cold day take-off conditions, which occur at −10°C, accounting the battery pack limit temperature, as shown on Fig. 13, to sufficiently cool the TMS 1.99kg/s air mass flow is chosen.

Accordingly, the coolant mass flow is 3.16kg/s, which is 34% lower than at ECS. The results are summarised on Table 7.

3.2.4. Surrounding air free convection impact

Centralised thermal management system

With the effect of free air convection, the thermal loads can be reduced as presented on Table 8 though not significantly. Batteries and generator loads showcase the highest reduction.

https://doi.org/10.1017/aer.2023.111 Published online by Cambridge University Press

Table 8. *Compartments heat loads with and without convection*

EPS compartment	Thermal load with convection (kW)	Thermal load without convection (kW)
eMotor	22.85	24
DC/AC inverter	5.37	6
Generator	52.47	55
AC/DC converter	9.62	11
Battery pack	45.9	48
DC/DC converter	14.55	16

Table 9. *Effect of convection on coolant mass flow*

Atmosphere conditions	CTMS $\dot{m}_{cool,conv}$ (kg/s)	CTMS $\dot{m}_{cool}$ (kg/s)	DTMS $\dot{m}_{cool}$ (kg/s)	DTMS $\dot{m}cool_{,conv}$ (kg/s)
ECS	1.68	1.68	4.78	4.78
HDTO	5.39	5.63	15.75	15.73
CDTO	1.11	1.11	3.16	3.14

Table 10. *Compartments thermal limits, power outputs and thermal loads*

TMS compartment	Decentralised TMS weight (kg)	Centralised TMS weight (kg)
$W_{HEX,wet,1}$	29.49	–
$W_{HEX,wet,2}$	26.8	–
$W_{HEX,wet,3\text{-}6}$	20.1	–
$W_{HEX,dry,1}$	27	–
$W_{HEX,dry,2}$	24.55	–
$W_{HEX,dry,3\text{-}6}$	14.8	–
$W_{HEX,wet,tot}$	136.72	127.42
$W_{HEX,dry,tot}$	125.2	116.6
W_{pipe}	4	2.75
W_{res}	2.56	1.99
W_{cool}	5.2	3.5
W_{pump}	85	22.56
$W_{wet,tot}$	233.48	158.22
$W_{dry,tot}$	219.4	143.9

In particular, on lower air mass flows the convection is more favorable as temperatures can reduce by 1.7%. On higher air mass flow, a 0.4% reduction is observed. On Table 9, the required coolant mass flows are compared for every atmosphere condition examined, and the most important reduction is observed at hot day conditions by 4.3%.

Decentralised thermal management system

On the decentralised system also, the free stream air convection effect is investigated. The results are presented on Table 9, and a 0.2–0.4% reduction on the required coolant mass flow is realised. Furthermore, the convection induces a higher impact on the decentralised system as further reduction is realised.

https://doi.org/10.1017/aer.2023.111 Published online by Cambridge University Press

3.3. Weight model results

3.3.1. TMS weight overall weight and breakdown

The weight calculations for both the decentralised and centralised TMS were conducted for the baseline model, which is designed at ECS conditions at 7°C. The weight breakdown and overall weight results are presented on Table 10 for both TMS architectures. Regarding the CTMS the total dry mass is 143.9kg, while the wet mass is 158.22kg, which induces a 9% increase. The DTMS dry mass is 219.4kg, while the wet mass is 6% more, at 233.48kg. The decentralised design's wet mass is 32.2% higher than the centralised configuration. Therefore, the inclusion of the wet mass for both architectures is crucial.

On Figs. 14 and 15 the weight breakdown for both arrangements by percentage is presented. The HEX's weight on the CTMS constitutes 80.5% of the whole weight while on the DTMS 58.6%. It is also worth noticing that the pump's weight is 36.4% on the DTMS due to the high coolant mass flow necessary. To elaborate, the pump's mass is 22.56kg on the centralised TMS, and 85kg on the decentralised TMS. The radically increased pump weight of the decentralised TMS stems from the high coolant mass flow, required to sufficiently cool the system. Furthermore, the required pumping power on the centralised configuration is 1,471.34W, while at the decentralised TMS is almost quadruple at 4,184.34W.

3.3.2. Pump weight variation

As illustrated above the pump weight especially on the decentralised TMS greatly affects the total mass, because of the high required coolant mass flow. Hence its design was investigated for the two alternative conditions. Sizing the pump of the centralised TMS during cold day takeoff conditions, would reduce its

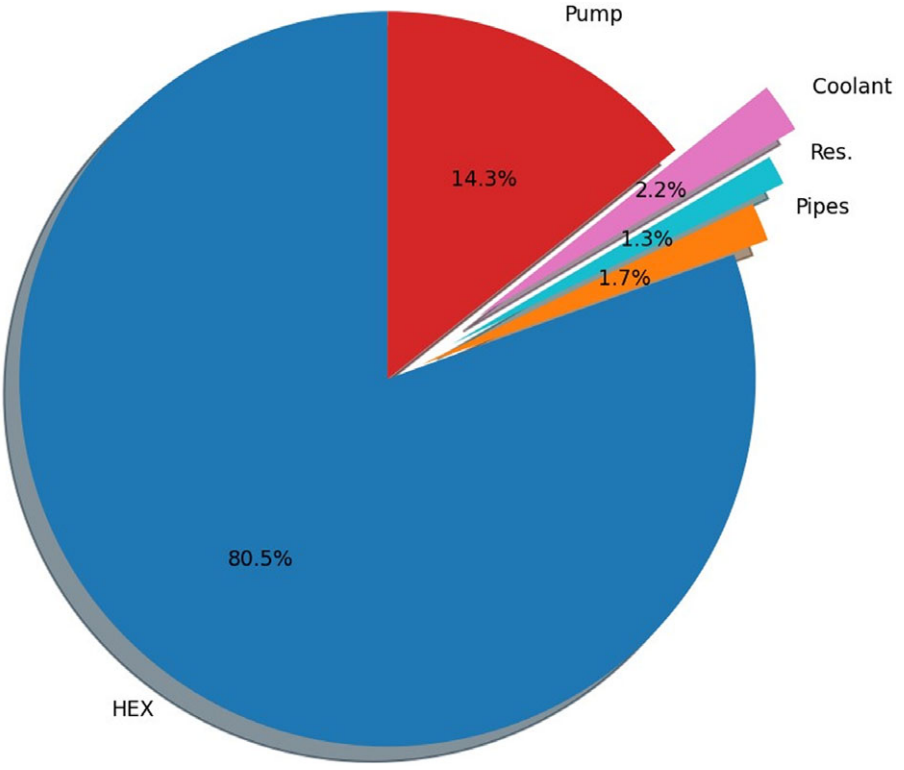

Figure 14. *CTMS weight breakdown.*

https://doi.org/10.1017/aer.2023.111 Published online by Cambridge University Press

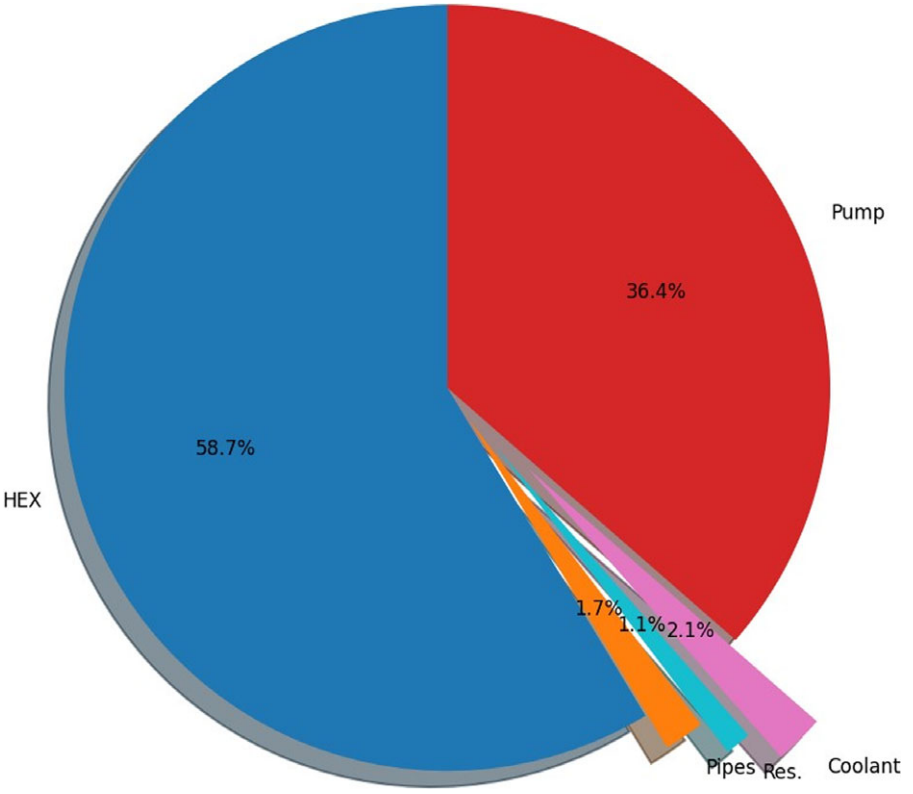

Figure 15. *DTMS weight breakdown.*

weight by 50%, at 13.22kg. However, at HDTO the weight is five times higher at 115.63kg. In reference to the decentralised TMS, at CDTO the pump's weight Is reduced by 40% at 52.36kg, while at HDTO the weight in increased at 477.39kg, by 82%. It is evidently presented on Table 11 for the centralised and decentralised TMS, respectively, that an increase in coolant mass flow radically increases the pump weight.

3.4. TMS design sensitivity analysis

In conclusion, the weight of DTMS architecture is substantially higher than the CTMS. Furthermore, the thermal modelling results indicate significant differentiation between these two architectures. The above prove that the effect of the number of heat exchangers introduced in the design should be explored. To elaborate, a tradeoff occurs between the number of TMS HEXs and the required air mass flow to cool them. In addition, the required heat transfer area is reduced for higher coolant mass flow. On Fig. 16 the impact on the whole wet weight is presented and it appears to be linear, as it increases with increasing HEX's number. On Fig. 17, the effect on required air mass flow is presented. At ECS and CDTO conditions, for the DTMS design the mass flow is almost equal while for the CMTS design a small variation is featured. On HDTO conditions, while the effect is still linear the gradient occurred is quite steep. The increase in HDTO conditions mass flow values highlight the importance of the ECS. The DTMS requires exponentially lower air. This effect renders the DTMS design appealing because higher air mass flow increases parasitic drag.

https://doi.org/10.1017/aer.2023.111 Published online by Cambridge University Press

Table 11. *Pump sizing variation with atmosphere conditions*

Atmosphere conditions	CTMS pump weight (kg)	CTMS pump power (W)	DTMS pump weight (kg)	DTMS pump power (W)
ECS	22.56	1,471.34	85	4,178.34
HDTO	115.63	4,926.63	477.39	13,777.5
CDTO	13.22	973.6	52.36	2,764.23

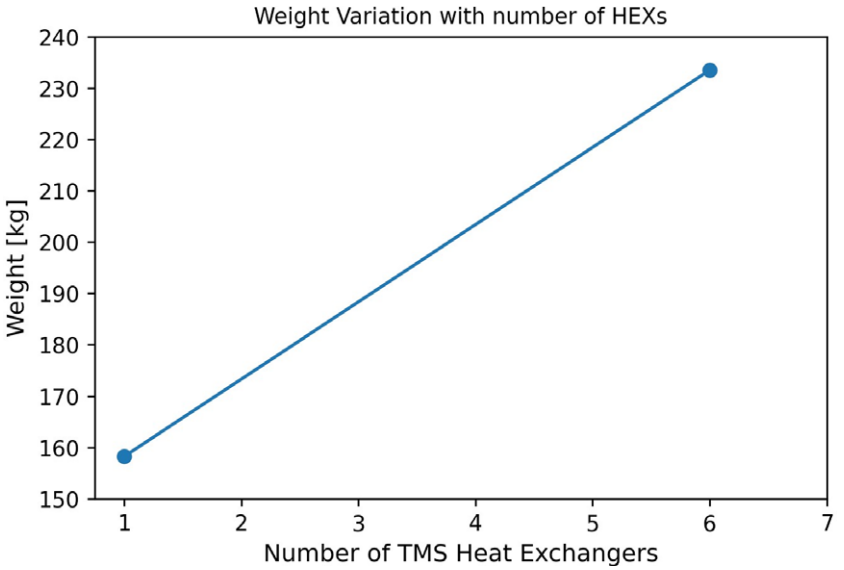

Figure 16. *Weight variation with number of HEXs.*

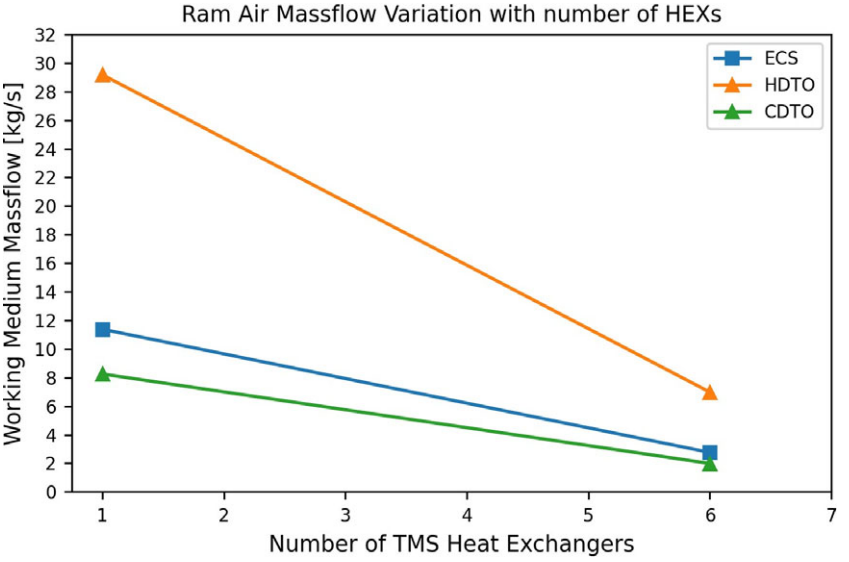

Figure 17. *Ram air massflow variation with number of HEXs.*

https://doi.org/10.1017/aer.2023.111 Published online by Cambridge University Press

3.5. Error propagation analysis

3.5.1. Method

Since many design parameters are not determined during the conceptual design phase of an aircraft, an uncertainty ($\delta x1, \delta x2, \ldots, \delta xn$) is considered to accompany design parameters ($x1, x2..xn$) deemed critical to the design. The formula and method used to examine uncertainty is presented on paper [21].

The variables investigated are the HEX surface, as it greatly impacts the TMS weight, the compact factor, the porosity and the HEX's material density. Furthermore, the hydraulic diameter, the length of pipes and the coolant mass flow were explored. Initial relative uncertainties for the design variables must

Table 12. *Uncertainties for design parameters*

Parameter	Value	Variable uncertainty	δx/x (%)
Compactness ratio β (m^2/m^3)	1,100	55	5
Material density ρ_{HEX} (kg/m^3)	2,700	135	5
Porosity factor σ	0.5	0.025	5
CTMS coolant mass flow (kg/s)	1.1682	0.0584	5
DTMS coolant mass flow (kg/s)	4.78	0.239	5
CTMS heat transfer area (m^2)	95	4.75	5
DTMS heat transfer $area_1$ (m^2)	22	1.1	5
DTMS heat transfer $area_2$ (m^2)	20	1	5
DTMS heat transfer $area_{3\text{-}6}$ (m^2)	15	0.75	5
CTMS pipe length (m)	54	2.7	5
DTMS pipe length (m)	58	2.9	5
Hydraulic diameter (mm)	18	0.9	5

Table 13. *Uncertainty propagation for final parameters, CTMS configuration*

	$\frac{\delta\beta}{\beta}$ (%)	$\frac{\delta\sigma}{\sigma}$ (%)	$\frac{\delta A_{HEX,1}}{A_{HEX,1}}$ (%)	$\frac{\delta\rho_{HEX}}{\rho_{HEX}}$ (%)	$\frac{\delta L}{L}$ (%)	$\frac{\delta\dot{m}_{coolant}}{\dot{m}_{coolant}}$ (%)	$\frac{\delta D_H}{D_H}$ (%)	Combined uncertainty (%)
$\frac{\delta V_{HX,CTMS}}{V_{HEX,CTMS}}$	± 5	–	± 5	–	–	–	–	± 7.07
$\frac{\delta\dot{Q}_{cool,CTMS}}{\dot{Q}_{cool,CTMS}}$	–	–	–	–	–	± 6.69	–	± 6.69
$\frac{\delta\upsilon_{coolant}}{\upsilon_{coolant}}$	–	–	–	–	–	± 5	± 10	± 11.18
$\frac{\delta Re}{Re}$	–	–	–	–	–	± 5	± 5	± 7.07
$\frac{\delta f}{f}$	–	–	–	–	–	± 5	± 5	± 7.07
$\frac{\delta P_{CTMS}}{P_{CTMS}}$	–	–	–	–	± 0.086	± 0.17	± 0.43	± 0.48
$\frac{\delta P_{pump,CTMS}}{P_{pump,CTMS}}$	–	–	–	–	± 0.104	± 0.31	± 0.104	± 0.35
$\frac{\delta V_{coolant}}{V_{coolant}}$	–	–	–	–	± 5	–	± 10	± 11.18
$\frac{\delta V_{res,CTMS}}{V_{res,CTMS}}$	–	–	–	–	± 2.74	–	± 1.37	± 3.07
$\frac{\delta W_{HEX,dry,CTMS}}{W_{HEX,dry,CTMS}}$	± 5	± 5	± 5	± 5	–	–	–	± 10
$\frac{\delta W_{HEX,wet,CTMS}}{W_{HEX,wet,CTMS}}$	± 5	± 4.14	± 5	± 4.56	–	–	–	± 9.37
$\frac{\delta W_{pipe,CTMS}}{W_{pipe,CTMS}}$	–	–	–	–	± 5	–	± 10	± 11.18
$\frac{\delta W_{pump,CTMS}}{W_{pump,CTMS}}$	–	–	–	–	–	± 6.57	–	± 6.57
$\frac{\delta W_{coolant}}{W_{coolant}}$	–	–	–	–	± 5	–	± 10	± 11.18
$\frac{\delta W_{res,CTMS}}{W_{res,CTMS}}$	–	–	–	–	± 1.29	–	± 0.64	± 1.44

https://doi.org/10.1017/aer.2023.111 Published online by Cambridge University Press

Table 14. *Uncertainty propagation for final parameters, DTMS configuration*

	$\frac{\delta\beta}{\beta}$ (%)	$\frac{\delta\sigma}{\sigma}$ (%)	$\frac{\delta A_{HEX,1}}{A_{HEX,1}}$ (%)	$\frac{\delta A_{HEX,2}}{A_{HEX,2}}$ (%)	$\frac{\delta A_{HEX,3}}{A_{HEX,3}}$ (%)	$\frac{\delta\rho_{HEX}}{\rho_{HEX}}$ (%)	$\frac{\delta L}{L}$ (%)	$\frac{\delta\dot{m}_{coolant}}{\dot{m}_{coolant}}$, (%)	$\frac{\delta D_H}{D_H}$ (%)	Combined uncertainty (%)
$\frac{\delta V_{HEX,\mathrm{DTMS},1-6}}{V_{HEX,\mathrm{DTMS},1-6}}$	± 5	–	–	± 5	–	–	–	–	–	± 7.07
$\frac{\delta\dot{Q}_{cool,\mathrm{DTMS},1}}{\dot{Q}_{cool,\mathrm{DTMS},1}}$	–	–	–	–	–	–	–	± 7.55	–	± 7.55
$\frac{\delta\dot{Q}_{cool,DTMS,2}}{\dot{Q}_{cool,DTMS,2}}$	–	–	–	–	–	–	–	± 7.78	–	± 7.78
$\frac{\delta\dot{Q}_{cool,DTMS,3-6}}{\dot{Q}_{cool,DTMS,3-6}}$	–	–	–	–	–	–	–	± 5.62	–	± 5.62
$\frac{\delta\upsilon_{coolant}}{\upsilon_{coolant}}$	–	–	–	–	–	–	–	± 5	± 10	± 11.18
$\frac{\delta Re}{Re}$	–	–	–	–	–	–	–	± 5	± 5	± 7.07
$\frac{\delta f}{f}$	–	–	–	–	–	–	–	± 5	± 5	± 7.07
$\frac{\delta P_{DTMS}}{P_{DTMS}}$	–	–	–	–	–	–	± 0.25	± 0.49	± 1.22	± 1.35
$\frac{\delta P_{pump,DTMS}}{P_{pump,DTMS}}$	–	–	–	–	–	–	± 0.92	± 2.77	± 0.92	± 3.06
$\frac{\delta V_{coolant}}{V_{coolant}}$	–	–	–	–	–	–	± 5	–	± 10	± 11.18
$\frac{\delta V_{res,DTMS}}{V_{res,DTMS}}$	–	–	–	–	–	–	± 3.39	–	± 1.7	± 3.8
$\frac{\delta W_{HEX,dry,1}}{W_{HEX,dry,2}}$	± 5	± 5	± 5	–	–	± 5	–	–	–	± 10
$\frac{\delta W_{HEX,dry,2}}{W_{HEX,dry,1}}$	± 5	± 5	–	± 5	–	± 5	–	–	–	± 10
$\frac{\delta W_{HEX,dry,3-6}}{W_{HEX,dry,3-6}}$	± 6.22	± 6.22	–	–	± 6.22	± 6.22	–	–	–	± 12.44
$\frac{\delta W_{HEX,wet,1}}{W_{HEX,wet,1}}$	± 5.01	± 5.01	± 4.14	–	–	± 4.58	–	–	–	± 9.4
$\frac{\delta W_{HEX,et,2}}{W_{HEX,wet,2}}$	± 5	± 5	–	± 4.15	–	± 4.58	–	–	–	± 9.4
$\frac{\delta W_{HEX,wet,3-6}}{W_{HEX,wet,3-6}}$	–	± 5	–	–	± 4.15	± 4.58	–	–	–	± 9.4
$\frac{\delta W_{pipe,DTMS}}{W_{pipe,DTMS}}$	–	–	–	–	–	–	± 0.57	–	± 10	± 10
$\frac{\delta W_{pump,DTMS}}{W_{pump,DTMS}}$	–	–	–	–	–	–	–	± 7.4	–	± 7.4
$\frac{\delta W_{coolant}}{W_{coolant}}$	–	–	–	–	–	–	± 5	–	± 10	± 11.18
$\frac{\delta W_{res,DTMS}}{W_{res,DTMS}}$	–	–	–	–	–	–	± 1.03	–	± 0.52	± 1.16

be determined, and are considered 5%. This value is selected as it an approximate practice occurring when working with at experimental data, and hence, the whole approach is viewed similarly to an experimental error propagation analysis. Variable uncertainties can be calculated afterwards, as presented on Table 12.

3.5.2. Results

The results of the propagation of uncertainties of the TMS weights and its compartments are demonstrated on Tables 13 and 14, for the centralised and decentralised architectures, respectively. It is apparent that the first row showcases the design variables whereas the first column indicates the parameters where uncertainties occur. Moreover, on Table 15 the uncertainties for the total wet and dry weight for both designs are presented in order to compare them efficiently.

Referring to the centralised design, it is observed on Table 13, that the design variables related to the HEX equally affect the HEX dry weight and volume, while HEX's wet weight is primarily influenced from the heat exchanger surface and compactness factor. Equally, as presented on Table 15, these variables affect equally the total dry and wet weight, though the material density features the highest

https://doi.org/10.1017/aer.2023.111 Published online by Cambridge University Press

Table 15. *Total weights uncertainty propagation for CTMS and DTMS architectures*

	$\frac{\delta\beta}{\beta}$ (%)	$\frac{\delta\sigma}{\sigma}$ (%)	$\frac{\delta A_{HEX,1}}{A_{HEX,1}}$ (%)	$\frac{\delta A_{HEX,2}}{A_{HEX,2}}$ (%)	$\frac{\delta A_{HEX,3}}{A_{HEX,3}}$ (%)	$\frac{\delta\rho_{HEX}}{\rho_{HEX}}$ (%)	$\frac{\delta L}{L}$ (%)	$\frac{\delta\dot{m}_{coolant}}{\dot{m}_{coolant}}$ (%)	$\frac{\delta D_H}{D_H}$ (%)	Combined uncertainty (%)
$\frac{\delta W_{CTMS,dry}}{W_{CTMS,dry}}$	± 4.05	± 4.05	± 4.05	–	–	± 5.4	± 1.37	± 1.02	± 0.011	± 9
$\frac{\delta W_{DTMS,dry}}{W_{DTMS,dry}}$	± 2.85	± 2.85	± 0.62	± 0.56	± 1.68	± 3.37	± 0.9	± 2.87	± 0.012	± 6.54
$\frac{\delta W_{CTMS,wet}}{W_{CTMS,wet}}$	± 4.03	± 4.03	± 4.03	–	–	± 4.92	± 1.67	± 0.94	± 0.86	± 8.5
$\frac{\delta W_{DTMS,wet}}{W_{DTMS,wet}}$	± 2.94	± 2.43	± 0.63	± 0.58	± 1.76	± 3.52	± 1.13	± 2.7	± 0.58	± 6.24

influence inducing a 5.4% and 4.92% error, respectively. In addition, the pipe length majorly affects the coolant weight and volume, with 5% error. In contrast it slightly influences both dry and wet total weight. The same can be concluded for the hydraulic diameter as it induces the lowest error. Hence, it equally features a high effect at volume and weight of the coolant, the coolant velocity and piping weight at 10%. The last variable examined, the coolant mass flow, induce higher impact at heat transfer and pump weight while it equally affects friction factor, Reynolds number and coolant velocity.

As presented on Table 14 for the DTMS design, the dry and wet weight as well as the volume of all the HEXs, indicate the same dependencies to these variables. The distinguishing feature of the DTMS appears at the HEXs on the motor loops, as they feature higher errors than the others, at 6.22%. Furthermore, their surface has a higher impact on the total dry and wet weight than the other HEXs', although the highest impact is introduced by the material density at 3.52%. The piping length and hydraulic diameter do not affect the total weight extensively. The piping length induces crucial error at coolant volume and weight at 5%. The hydraulic diameter instigates the same magnitude of error at volume and weight of the coolant, the coolant velocity and piping weight. Furthermore, the coolant mass flow, features a lower error at heat transfer of each HEX, though notable, compared to the centralised TMS, and introduces a 2.87% and 2.7% error at dry and wet weight sequentially.

4.0. Conclusions and future work

This research investigates the TMS design for a series hybrid aircraft propulsion architecture. To elaborate, two alternative configurations are examined: a centralised and a decentralised TMS, aiming to minimise their total weight, in order to induce lower impact on the aircraft's total weight. For the research goals a computational tool was developed for the thermal and weight sizing of the TMS. The analysis conducted resulted in the following conclusions:

- The decentralised configuration results in lower temperature fields for all components compared to the centralised configuration. Furthermore, the temperature curve features exponential trend with air mass flow. The equation of these two values could be shaped as: $T = a \cdot e^{m_{air}},\ a \in R$.
- Battery pack's assumed temperature limit at 40°C severely influence the TMS dimensioning. At HDTO conditions to produce a viable design for both architectures, their limit temperature must be increased to 50°C.
- A tradeoff occurs between heat transfer area and the air and coolant mass flow. Increasing coolant mass flow reduces the required heat transfer surface area. The CTMS requires smaller coolant mass flow at 1.1682kg/s, while the DTMS requires 4.78kg/s. However, in order to cool the HEXs of the decentralised TMS less air mass flow is necessary, about 75%, for all atmospheric conditions examined. Furthermore, the necessary heat transfer area of the CTMS in 95m^2, while for the DTMS is 102m^2. Their deviation is 6.9%.

https://doi.org/10.1017/aer.2023.111 Published online by Cambridge University Press

- The pump's weight at CDTO would be reduced by approximately 40%, while at HDTO conditions it would increase by 80%. This highlights the adverse effect of coolant mass flow in pump's weight.
- For both configurations, the HEXs' weight is equally influenced by porosity, heat transfer area and compactness ratio, with 5% error. In addition, the error propagation analysis indicates that the total weight is majorly influenced by the HEX's material density, as it induces an error of 4.92% and 3.52% for the centralised and decentralised TMS, respectively. Subsequently lighter materials than aluminum could further reduce the weight. The total weight is also influenced by the HEX surface.
- The decentralised TMS weighs 233.48kg, which is 32.2% more than the centralised TMS (158.22kg) weight. Furthermore, the inclusion of the wet weight is illustrated as it is 6% and 9% increase in the decentralised and centralised TMS dry weight, respectively.

The discrepancy between the wet and dry weight, prove that the coolant mass impacts the weight. In this direction, a mixed TMS architecture, employing a liquid in combination with air or alternative solution (i.e. based on phase change solutions) attached to the batteries, could reduce the weight. The same benefit could be induced by constructing the HEXs from a lighter material than aluminum. Furthermore, including atmosphere temperatures higher than 40°C and lower than −10°C, would provide a more thorough TMS design exploration.

References

[1] Rao, A.G., Yin, F. and Werij H.G. Energy transition in aviation: The role of cryogenic fuels, *Aerospace*, 2020, **7**, (12), p 181.

[2] Epstein, A.H. and O'Flarity, S.M. Considerations for reducing aviation's CO2 with aircraft electric propulsion, *J. Propul. Power*, 2019, **35**, (3), pp 572–582.

[3] Nasoulis, C.P., Protopapadakis, G., Ntouvelos, E.G., Gkoutzamanis, V.G. and Kalfas, A.I. Environmental and techno-economic evaluation for hybrid-electric propulsion architectures, *Aeronaut. J.*, 2023, pp 1–23

[4] Gkoutzamanis, V., Kavvalos, M., Srinivas, A., Mavroudi, D., Korbetis, G., Kyprianidis, K. and Kalfas, A. Conceptual design and energy storage positioning aspects for a hybrid-electric light aircraft, *J. Eng. Gas Turbines Power,* 2021, **143,** (9).

[5] Voskuijl, M., Van Bogaert, J. and Rao, A.G. Analysis and design of hybrid electric regional turboprop aircraft, *CEAS Aeronaut J.,* 2018, **9**, pp 15–25.

[6] Clark, R.A., Shi, M., Gladin, J. and Mavris, D. Design and analysis of an aircraft thermal management system linked to a low-bypass ratio turbofan engine, *J. Eng. Gas Turbines Power*, 2022, **144**, (1).

[7] Coutinho, M., Bento, D., Souza, A., Cruz, R., Afonso, F., Lau, F., Suleman, A., Barbosa, R.F., Gandolfi, R., Affonso, W.J., Odaguil, F.I.K., Westin, M.F., Dos Reis, R.J.N. and Da Silva, C.R.I. A review on the recent developments in thermal management systems for hybrid-electric aircraft, *Appl. Therm. Eng.*, 2023, **227,** (120427).

[8] Rendón, M.A., Assato, M., Martins, V.A.C., Hallak, P.H., Altgott, A.S., Graça, R., Landy, Z., Oliveira, N.L. and Delmonte, R.G.P. Design method and performance analysis of a hybrid-electric power-train applied in a 30-passenger aircraft, *J. Cleaner Prod.*, 2022, **339**, p 130560.

[9] Lents, C. E. and Hardin, L. W. Fuel Burn and Energy Consumption Reductions of a Single-Aisle Class Parallel Hybrid Propulsion System, AIAA Propulsion and Energy 2019 Forum, AIAA Paper 2019-4396, 2019.

[10] Rheaume, J.M., Macdonald, M. and Lents, C.E. Commercial hybrid electric aircraft thermal management system design, simulation, and operation improvements, AIAA Propulsion and Energy 2019 Forum, AIAA Paper 2019-4492, 2019.

[11] Lents, C.P., Hardin, L., Rheaume, J. and Kohlman, L. Parallel hybrid gas electric geared turbofan engine conceptual design and benefits analysis, 52nd AIAA/SAE/ASEE Joint Propulsion Conference, AIAA Paper 2016-4610, 2016

[12] Fefermann, Y., Maury, C., Zarati, K., Salanne, J.P., Pornet, C., Thoraval, B. and Isikveren, A. Hybrid-electric motive power systems for commuter transport applications, 30th International Council of the Aeronautical Sciences, 2016.

[13] BROWN, G.V. Weights and efficiencies of electric components of a turboelectric aircraft propulsion system, 49th AIAA Aerospace Sciences Meeting including the New Horizons Forum and Aerospace Exposition, January 2011, 2012.

[14] Harish, A., Gladin, J. and Mavris, D. Architecture Evaluation of a Single-aisle Turbo-electric Aircraft with One Engine Inoperative Considerations, AIAA Paper 2018-3838, 2018.

[15] Perullo, C., Shi, M., Cinar, G., Alahmad, A., Sanders, M. and Mavris, D.N. An update on sizing and performance analysis of a hybrid turboelectric regional jet for the NASA ULI program, 2020 AIAA/IEEE Electric Aircraft Technologies Symposium (EATS), 2020.

[16] Affonso, W., Tavares, R., Barbosa, F., Gandolfi, R., dos Reis, R., da Silva, C., Kipouros, T., Laskaridis, P., Enalou, H. and Chekin A. System architectures for thermal management of hybrid-electric aircraft - FutPrInt50, *IOP Conf. Ser. Mater. Sci. Eng.*, 2022, **1226**, (1), Paper 012062.

https://doi.org/10.1017/aer.2023.111 Published online by Cambridge University Press

[17] Van Heerden, A.S.J., Judt, D.M., Jafari, S., Lawson, C.P., Nikolaidis, T. and Bosak, D. Aircraft thermal management: Practices, technology, system architectures, future challenges, and opportunities, *Progr. Aerospace Sci.*, 2022, **128**, p 100767.
[18] Freeman, J., Osterkamp, P.G., Green, M., Gibson, A. and Schiltgen, B.T. Challenges and opportunities for electric aircraft thermal management, *Aircraft Eng. Aerospace Technol.*, 2014, **86**, (6), pp 519–524.
[19] Schnulo, S.L., Chin, J.C., Smith, A.D. and Paul-Dubois-Taine. Steady state thermal analyses of Sceptor X-57 wingtip propulsion, AIAA 2017-3783. 17th AIAA Aviation Technology, Integration and Operations Conference, June 2017.
[20] Kellermann, H., Lüdemann, M., Pohl, M. and Hornung, M. Design and optimization of ram air-based thermal management systems for hybrid-electric aircraft, *Aerospace*, 2021, **8**, (1), p 3.
[21] Gkoutzamanis, V.G., Valsamis Mylonas, O.S. and Kalfas, A.I. Parametric analysis for on-board thermal regulation in a hybrid-electric aircraft, Proceedings of the ASME Turbo Expo 2022: Turbomachinery Technical Conference and Exposition. Volume 1: Aircraft Engine; Ceramics and Ceramic Composites. Rotterdam, Netherlands. June 13–17, 2022. V001T01A029. ASME.
[22] Gkoutzamanis, V.G., Tsentis, S.E., Valsamis Mylonas, O.S., Kalfas, A.I., Kyprianidis, K.G., Tsirikoglou, P. and Sielemann, M. Thermal management system considerations for a hybrid-electric commuter aircraft, *J. Thermophys. Heat Transfer,* 2022, **36**, (3), pp 466–484.
[23] Chapman, J.W., Hasseeb, H. and Schnulo, S. Thermal management system design for electrified aircraft propulsion concepts, 2020 AIAA/IEEE Electric Aircraft Technologies Symposium (EATS), 2020.
[24] Abolmoali, P.C., Donovan, A.B., Patnaik, S.S., Mccarthy, P., Dierker, D., Jones, N. and Buettner, R. Integrated propulsive and thermal management system design for optimal hybrid electric aircraft performance, Propulsion and Energy 2020 Forum, AIAA Paper 2020-3557, 2020.
[25] Roumeliotis, I., Castro, L., Jafari, S., Pachidis, V., De Riberolles, L., Broca, O. and Unlu D. Integrated systems simulation for assessing fuel thermal management capabilities for hybrid-electric rotorcraft, Proceedings of the ASME Turbo Expo 2020: Turbomachinery Technical Conference and Exposition, Paper ASME GT2020-15107, 2020.
[26] Brelje, B.J., Jasa, J.P., Martins, J. and Gray J. Development of a Conceptual-Level Thermal Management System Design Capability in OpenConcept. NATO TR STO-MP-AVT-323, 2019.
[27] Shi, M., Sanders, M., Alahmad, A., Perullo, C., Cinar, G. and Mavris, D.N. Design and analysis of the thermal management system of a hybrid turboelectric regional jet for the NASA ULI program, 2020 AIAA/IEEE Electric Aircraft Technologies Symposium (EATS), 2020.
[28] Kellermann, H., Habermann, A.L. and Hornung, M. Assessment of aircraft surface heat exchanger potential, Aerospace 2020, **7**, 1.
[29] Wu, W., Wang, S, Wu, W., Chen, K., Hong, S. and Lai, Y. A critical review of battery thermal performance and liquid based battery thermal management, *Energy Convers. Manag.*, 2019, **182**, pp 262–281.
[30] Sheng, L., Zhang, H., Zhang, Z. Su, L. and Zhang, Z. Lightweight liquid cooling based thermal management to a prismatic hard-cased lithium-ion battery, *Int. J. Heat Mass Transfer*, 2021, **170**, p 120998.
[31] Zhi, M., Fan, R., Yang, X., Zheng, L., Yue, S., Liu, Q. and He, Y. Recent research progress on phase change materials for thermal management of lithium-ion batteries, *J. Energy Storage*, 2022, **45**, p 103694, ISSN 2352-152X.
[32] Yetik, O., Yilmaz, N. and Karakoc, T.H. Computational modeling of a Lithium-Ion battery thermal management system with Al_2O_3-based nanofluids, *Int. J. Energy Res.*, 2021, **45**, (9), pp 13851–13864.
[33] Zohuri, B. *Compact Heat Exchangers*, Springer Nature, 2017, Switzerland, pp 19–183, Chap. 2–3.
[34] London, A.L.M. and Kays, W. *Compact Heat Exchangers*, Springer Nature, 2017, Switzerland, pp 19–183, Chap. 2–3.
[35] Hein, L.L. and Mortean M.V.V. Theoretical and experimental thermal performance analysis of an additively manufactured polymer compact heat exchanger, *Int. Commun. Heat Mass Transfer,* 2021, **124,** p 105237.
[36] Krishna, K.R., Vasu, V. and Kumar, A.C.S. Application of nanofluids in thermal design of compact heat exchanger, *Int. J. Nanotechnol. Appl.*, 2008, **2**, (1), pp 75–87. ISSN 0973-631X.
[37] Ning, J., Wang, X., Sun, Y., Zheng, C., Zhang, S., Zhao, X., Liu, C. and Yan, W. Experimental and numerical investigation of additively manufactured novel compact plate-fin heat exchanger, *Int. J. Heat Mass Transfer*, 2022, **190**, p 122818.
[38] Moran, S. Pump Sizing: Bridging the Gap Between Theory and Practice. CEP, American Institute of Chemical Engineers, 2016.
[39] Zhou, Z., Li, G. and Zhang, Y. Wide working temperature range rechargeable Lithium–Sulfur batteries: A critical review, *Adv. Funct. Mater.,* 2021, **31**, p 2107136.

Cite this article: Potamiti M., Gkoutzamanis V.G. and Kalfas A.I. Thermal management system design for a series hybrid-electric propulsion architecture. *The Aeronautical Journal*, https://doi.org/10.1017/aer.2023.111